Acta Oceanol. Sin., 2024, Vol. 43, No. 2, P. 58–66
https://doi.org/10.1007/s13131-023-2222-6
http://www.aosocean.com
E-mail: ocean2@hyxb.org.cn

Effects of shore-normal coastal structure on medium- to long-term embayed shoreline evolution

Jitao Yu[1, 2], Yuanting Ding[3], Pei Liu[1, 2], Renfu Fan[1, 2], Lin Zhang[1, 2*]

[1] Hainan Academy of Ocean and Fisheries Sciences, Haikou 571126, China

[2] Yazhou Bay Innovation Institute, Hainan Tropical Ocean University, Sanya 572025, China

[3] School of Geography and Environmental Sciences, Hainan Normal University, Haikou 571158, China

Received 2 February 2023; accepted 23 June 2023

Abstract

Based on high-tide shoreline data extracted from 87 Landsat satellite images from 1986 to 2019 as well as using the linear regression rate and performing a Mann-Kendall (M–K) trend test, this study analyzes the linear characteristics and nonlinear behavior of the medium- to long-term shoreline evolution of Jinghai Bay, eastern Guangdong Province. In particular, shoreline rotation caused by a shore-normal coastal structure is emphasized. The results show that the overall shoreline evolution over the past 30 years is characterized by erosion on the southwest beach, with an average erosion rate of 3.1 m/a, and significant accretion on the northeast beach, with an average accretion rate of 5.6 m/a. Results of the M–K trend test indicate that significant shoreline changes occurred in early 2006, which can be attributed to shore-normal engineering. Prior to that engineering construction, the shorelines are slightly eroded, where the average erosion rate is 0.7 m/a. However, after shore-normal engineering is performed, the shoreline is characterized by significant erosion (3.2 m/a) on the southwest beach and significant accretion (8.5 m/a) on the northeast beach, thus indicating that the shore-normal engineering at the updrift headland contributes to clockwise shoreline rotation. Further analysis shows that the clockwise shoreline rotation is promoted not only by longshore sediment transport processes from southwest to northeast, but also by cross-shore sediment transport processes. These findings are crucial for beach erosion risk management, coastal disaster zoning, regional sediment budget assessments, and further observations and predictions of beach morphodynamics.

Key words: shoreline rotation, non-linear behavior, longshore sediment transport, cross-shore sediment transport, embayed beach, coastal structure

Citation: Yu Jitao, Ding Yuanting, Liu Pei, Fan Renfu, Zhang Lin. 2024. Effects of shore-normal coastal structure on medium- to long-term embayed shoreline evolution. Acta Oceanologica Sinica, 43(2): 58–66, doi: 10.1007/s13131-023-2222-6

1 Introduction

Sandy coasts are extremely dynamic geomorphic systems, and their shorelines evolve due to the coupling of different forcing mechanisms (e.g., wind, waves, and tides) as well as their interaction with natural or artificial coastal landforms. This implies that shoreline changes occur over different time-scales, including high-frequency changes related to daily fluctuations in wave energy and the associated processes, rapid changes due to individual storm events over only several days, gradual changes due to seasonal wave climate, as well as interannual and interdecadal changes associated with climate oscillations. Therefore, the shoreline position observed at any specified time presents a summary of the combined actions of these short- and long-term processes, which renders it difficult to determine whether these processes are independent or dependent on shoreline changes (Dolan et al., 1991).

However, cross-shore and long-shore sediment transport processes must be considered in most investigations pertaining to coastal morphodynamics (Hansen and Barnard, 2010; Harley et al., 2011, 2015). Under energetic wave conditions, sediment is eroded from the beach face and deposited offshore. Calm wave conditions allow the sediment to be returned to subaerial beaches. This cross-shore process is the result of sediment exchange between subaerial beaches and subaqueous bars, and typically manifests as shoreline oscillations (Short and Trembanis, 2004; Harley et al., 2011). Longshore sediment transport typically occurs on sandy coasts, particularly on embayed beaches. Reverse longshore sediment exchange occurring between two opposite ends of an embayed beach is the classic and generally accepted beach rotation model, which is defined by Short and Masselink (1999), and this reversal is mainly due to variations in wave direction (da Fontoura Klein et al., 2002; Masselink and Pattiaratchi, 2001; Thomas et al., 2011b). Some studies suggested that this reversal is related to changes in large-scale climatic conditions, such as the El Niño-Southern Oscillation (Short et al., 2000; Ranasinghe et al., 2004) and the North Atlantic Oscillation (Thomas et al., 2011b). Ranasinghe et al. (2004) examined the relationship among the Southern Oscillation index, wave climate, and beach rotation on the southern and central coasts of Australia; and showed a clockwise shoreline rotation during El Niño events and an anti-clockwise rotation during La Niña events. In fact, other factors may result in shoreline rota-

Foundation item: The National Nature Science Foundation of China under contract No. 42071007; the Nature Science Foundation of Hainan Province under contract Nos 422RC665, 421QN0883, and 423RC553.
*Corresponding author, E-mail: adela0531@126.com

tion, including the migration patterns of nearshore mudbanks (Anthony et al., 2002), beach diminution and migration associated with spit collapse (Thomas et al., 2011a), and large-scale bathymetric changes (Hansen and Barnard, 2010). Recently, Harley et al. (2011) reported that elucidating beach rotation purely based on the longshore sediment transport is extremely simplistic, and thus suggested that the longshore variability in the cross-shore sediment transport process might be a more significant indicator. Harley et al. (2015) identified the importance of wave exposure and cross-shore processes in beach rotation. Notably, shoreline rotation can occur not only on natural embayments, but also on artificial embayments. Ojeda and Guillén (2008) investigated shoreline dynamics in three artificially embayed micro-tidal beaches in Barcelona City based on Argus video images; and indicated that beach rotation was controlled by both natural processes and anthropogenic actions.

Embayed sandy beaches are the predominant coastal landforms along the South China coastline (Li and Chen, 2006; Yu and Chen, 2011); however, few studies have focused on shoreline rotation, which is mainly attributed to the absence of medium-term to long-term beach observation data, such as data from continuous, long-term beach profile observations (Ranasinghe et al., 2004; Harley et al., 2011) or high-frequency video shoreline monitoring (Ojeda and Guillén, 2008). Therefore, high-tide shorelines extracted from Landsat series satellite images from 1986 to 2019 at Jinghai Bay in eastern Guangdong are used in this study as a proxy to report the embayed shoreline rotation caused by a shore-normal structure. By identifying when and how the shore-normal structure affects medium-term to long-term shoreline evolution, this study attempts to clarify the dominance of cross-shore and longshore sediment transport processes associated with shoreline rotation in Jinghai Bay. The results obtained are important for beach erosion risk management, hazard zoning, regional sediment budget assessments, and further observations and predictions of coastal morphodynamics.

2 Study area description

Jinghai Bay, which is a typical embayed sandy beach in South China, is located on the east coast of Jieyang City, Guangdong Province (22°58′25.2″–23°00′21.3″ N and 116°30′50.9″–116°32′23.6″E; Fig. 1). It is open to the southeast, and water from Shishi Lake in the northwest flows into the head of the bay. Owing to low runoffs and sediment concentrations, the effect of terrestrial sediment supply on the evolution of the bay is limited. Sediment samples obtained from the upper and lower intertidal zones of six beach profiles during six beach observations from 2015 to 2019 indicated that the beach was mainly composed of medium sand. The average sediment particle sizes Φ were 1.26 and 1.40 in the upper and lower intertidal zone, respectively. The average annual wave height was 1.5–2.0 m within a 6.2–6.5 s period. The dominant waves were from the SE, NE, and E, whereas the energetic waves were from the NE (Ji et al., 2016). Irregular diurnal tides, with an average tidal range of less than 1m, dominated the study area. Therefore, Jinghai Bay is classified as a micro-tidal wave-dominated coast.

Jinghai Bay has been subjected to various forms of human intervention. For example, the construction of a shore-normal structure (breakwater engineering) for the Huilai Power Plant began at the updrift headland in 2005 and was completed in 2008. The breakwater extends 1 200 m seaward from the updrift headland in the SSW direction (Fig. 2). Additionally, the central beach of Jinghai Bay (Fig. 1, P04–P05) was developed as a bathing beach, whereas wind turbines and high-level shrimp ponds were constructed behind the exposed southwest coastal segment of the bay.

3 Data description and methods

3.1 *Dataset*

A total of 87 remote sensing images from the Landsat series satellites from 1986 to 2019 were used to extract high-tide shorelines and construct a time series of shoreline positions (Fig. 3). These images were obtained using the TM sensor of Landsat 5, ETM+ sensor of Landsat 7, and OLI sensor of Landsat 8, among which 29, 31, and 27 images were obtained using the TM, ETM+, and OLI sensors, respectively. A spatial resolution of 30 m was used. These images were downloaded from the Geospatial Data Cloud website (http://www.gscloud.cn) and the United States Geological Survey website (https://earthexplor.usgs.gov). The additional data in this study included six field observations of six shore-normal beach profiles along the coastline of Jinghai Bay from 2015 to 2019. The high-tide shoreline positions obtained from the field measurements were mainly used to evaluate the accuracy of the shorelines extracted from the remote sensing images. Field observations were conducted on August 8, 2015; August 8, 2016; August 2, 2017; April 21, 2019; August 11, 2019; and November 13, 2019. During field observations, a total station in 2015 and an RTK-GPS from 2016 to 2019 were utilized to measure the morphological changes in the six beach profiles based on the China Geodetic Coordinate System 2000. Cross-shore measurements for each profile were commenced at a fixed backshore benchmark and ended at the deepest reachable location below the low-water line on the day of observation. One surficial sediment sample was obtained from each upper and lower intertidal profile, and 72 samples were obtained from six field observations.

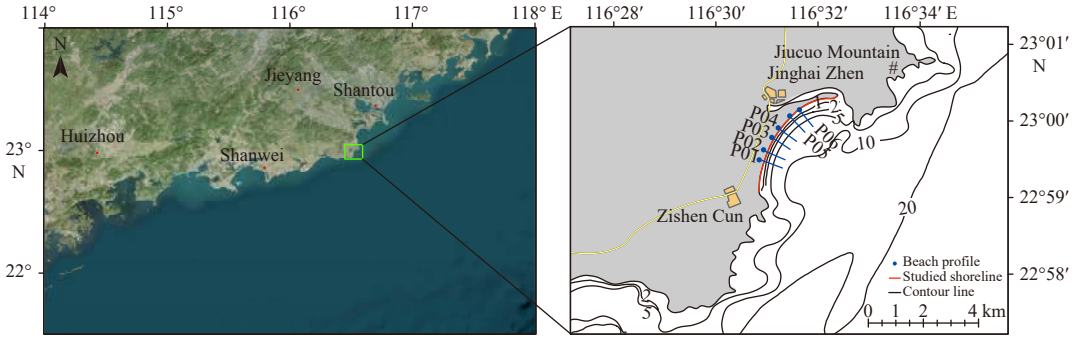

Fig. 1. Location of the study area, its bathymetric contours, and the measured beach profiles.

Fig. 2. Planform of Jinghai Bay: Before (a) and after construction of shore-normal breakwater (b).

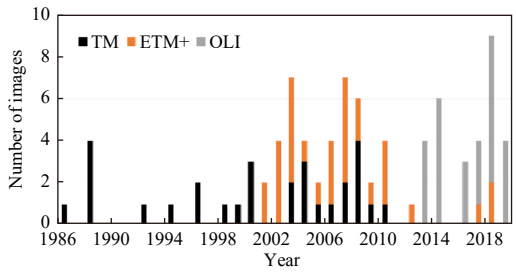

Fig. 3. Landsat series satellite images used in this study.

3.2 *Methods*

3.2.1 *High-tide shoreline extracted from Landsat images and accuracy evaluation*

Because of the highly dynamic nature of the sandy shoreline, the high-tide shoreline is typically extracted via manual visual interpretation based on the difference in sand color between dry subaerial beaches and periodic wet intertidal beaches (Del Río et al., 2013; Benkhattab et al., 2020; Zhu et al., 2022). First, the available images were preprocessed, including clipping, radiometric calibration, and atmospheric correction, using ENVI 5.3. Next, on the ArcGIS platform for processing the TM and ETM+ images, the fifth, fourth, and third bands were defined as R (red), G (green), and B (blue) respectively, and the high-tide shoreline was extracted based on false color synthesis. Meanwhile, for the OLI images, the combination of the fourth, fifth, and sixth bands was used to extract the shoreline.

The root-mean square error (RMSE) is typically used to measure accuracy (Hou et al., 2016; Zhu et al., 2022), and was defined by Maune (2007) as the squared difference between the dataset coordinate values and the coordinates from an independent source of higher accuracy for identical points. Hence, in this study, four remote sensing images were obtained at imaging times that were the closest to the four shoreline observation times. The imaging times for these four images were December 9, 2016; October 25, 2017; September 29, 2019; and November 16, 2019. Hence, the calculated RMSE values were 30.3 m, 26.2 m, 20.9 m, and 19.8 m, respectively, which were within one pixel. In particular, owing to the minimum time interval (3 days), the RMSE value was the lowest between the shoreline data measured on November 13, 2019, and the remote sensing shoreline data obtained on November 16, 2019. Similar to the method of Zhu et al. (2022), the visual interpretation method for extracting the high-tide shoreline is reliable.

3.2.2 *Linear regression rate method based on single-transect method*

Using the ArcGIS software, users can use the digital shoreline analysis system (DSAS) to create transects separated by a specified distance (Thieler et al.,2017). Along each transect, various statistical indicators such as the end-point rate (EPR) and linear regression rate (LRR) can be used to calculate the shoreline change rate and its uncertainty. In this study, 121 transects with 50 m spacing were created from southwest to northeast along the coastline of Jinghai Bay, which were labeled T01–T121, and each transect contained 87 shoreline positions. To minimize the effects of outliers caused by short-term processes or extreme events on shoreline changes over the past 30 years, the LRR was used to calculate the shoreline change rate. Thus, the erosion or accretion conditions and the spatial variation in the shoreline change rate in Jinghai Bay can be estimated.

3.2.3 *Mann–Kendall (M–K) trend test*

When calculating the shoreline change rate, the underlying assumption of linear indicators (the EPR and LRR) is that the shoreline movement is constant and uniform, i.e., the shoreline change is considered to be linear. However, this is typically not the case in reality because of the inherent variability of shorelines, occasional extreme events, or human activity (Fenster and Dolan, 1994). To investigate the nonlinear behavior of shoreline evolution (e.g., trend reversal and erosion/accretion acceleration or deceleration) and further relate it to potential causes, the M–K trend test was performed to analyze the shoreline position data for each transect and to evaluate the linear or nonlinear behavior. The M–K trend test is a rank-based non-parametric test (Mann, 1945; Kendall, 1975), which can be used to effectively evaluate the long-term change trend (Wei, 2007). It does not require time-series data with a particular distribution (e.g., a normal distribution) and is less affected by outliers. Applying this method to shoreline studies and comparing with the polynomial model shows shat it allows significant trend changes and the time of changes to be easily observed based on its significance test (Zhu et al., 2022). The calculation procedure for the M–K trend test is as follows:

For a time series $x_k(k = 1,2,\cdots,n)$, the univariate M–K statistic is expressed as

$$s_k = \sum_{i=1}^{k} r_i \quad (2 \leqslant k \leqslant n), \tag{1}$$

in which

$$r_i = \begin{cases} +1 & \text{if } x_i > x_j \\ 0 & \text{otherelse} \end{cases} (j = 1, 2, \cdots, i), \quad (2)$$

The statistic index UF_k is expressed as

$$UF_k = \frac{[s_k - E(s_k)]}{\sqrt{\mathrm{Var}(s_k)}} \quad (k = 1, 2, \cdots, n), \quad (3)$$

in which $E(s_k) = n(n+1)/4$ and $\mathrm{Var}(s_k) = n(n-1)(2n+5)/72$.

In the reverse order of the time series x_n, x_{n-1}, ···, x_1, the procedure above is repeated, and $UB_k = -UF_k (k = n, n-1, \cdots, 1)$ and $UB_n = 0$ are set. This yields the statistical index UB.

A positive UF or UB value indicates a positive trend, whereas a negative UF or UB value indicates a negative trend. For the two-sided test, the null hypothesis of no trend is rejected at a significance level of p. In this study, $p = 0.01$ was used to evaluate the significance of the tested shoreline trend.

4 Results

4.1 *Shoreline changes over past 30 years*

Figure 4 shows the shoreline advance and retreat rates along Jinghai Bay calculated based on the LRR from 1986 to 2019. As shown, the southwest segment including transects from T01 to T73 eroded at an average erosion rate of 3.1 m/a, and a maximum erosion rate was indicated on transect T25 (4.6 m/a). However, the northeast segment including transects from T74 to T121 accreted at an average accretion rate of 5.6 m/a, and a maximum accretion rate was indicated on transect T121 (9.6 m/a). A clear inverse relationship was shown between erosion in the southwest coastal segment and accretion in the northeast segment, thus indicating that shoreline rotation occurred along the coastline of Jinghai Bay. As shown in Fig. 4, the rotation point was located between transects T73 and T74.

4.2 *Shoreline trend changes induced by shore-normal structure*

To comprehensively understand the trend characteristics and variability of the shorelines on 121 transects from southwest to northeast along the coastline of Jinghai Bay over the past 30 years, every 10 transects was sequentially segmented into one group, which resulted in 12 groups. The M–K trend test results for all transects of the Jinghai Bay shoreline position data are shown in Fig. 5. Figures 5a–c show that after 2001, shorelines on 30 transects of the southwest beach showed an increasingly significant erosion trend (at the 0.01 significance level), whereas the shorelines indicated a slight but insignificant erosion trend in the preceding period. Figures 5d–g indicate that the shorelines on the 40 transects of the central beach were slightly eroded or stable before 2005. After 2005, the shoreline erosion trend became significant, but the recent erosion trend declined gradually from southwest to northeast. Figures 5h–l show that beginning from 2005, shorelines on 51 transects of the northeast beach began to show significant trend changes, i.e., from slight erosion, accretion, or a relatively stable state (not exceeding the significance level of 0.01) in the early stage to the accretion state, and the time at which significant accretion occurred was inconsistent. For example, some transects (Figs 5j and 5k) began to significantly accrete in 2006–2007, whereas other transects began in 2018 (Fig. 5h). The aforementioned analysis results indicate that the shore-normal structure significantly affect the shoreline evolution of Jinghai Bay.

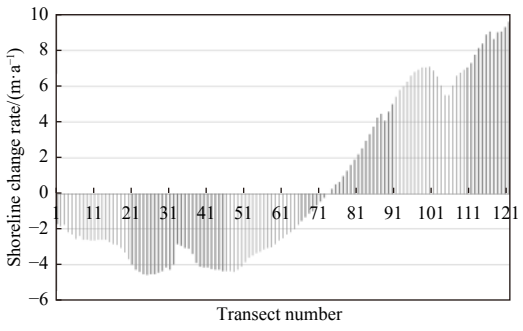

Fig. 4. Shoreline change rates on 121 transects generated at 50 m intervals (1986–2019).

4.3 *Shoreline advance and retreat before and after shore-normal engineering*

For a comparative evaluation of the shoreline variability before and after the construction of the shore-normal structure, based on the results of Section 4.2, the time at which significant erosion or accretion occurred on 121 transects was identified from Fig. 5. Subsequently, all the times were averaged, i.e., the times at which the shore-normal structure began to significantly affect the shoreline evolution of Jinghai Bay. The average time obtained was September, 2006, thus indicating that the coastline began to respond significantly to coastal engineering one year after its construction. Based on this identified average time, the time series of the shoreline position data from Jinghai Bay were categorized into two periods: before and after the construction of the shore-normal structure (1986–2005 and 2006–2019). The erosion and accretion rates in these two periods were calculated using the linear regression method, and the results are shown in Fig. 6.

As shown in Fig. 6a, before the construction of the normal-shore structure, transects T01–T93 eroded at an average erosion rate of 0.9 m/a, and the maximum erosion occurred on transect T20 at an erosion rate of 2.0 m/a. However, transects T94–T104 accreted at an average accretion rate of 0.6 m/a, and the maximum accretion occurred on transect T100 at an accretion rate of 0.9 m/a. In addition, transects T105–T121 eroded at an average erosion rate of 0.5 m/a, and the maximum erosion occurred on transects T111 and T112 at a rate of 1.1 m/a. In general, the change in shorelines in the period 1986–2005 was characterized by slight erosion at an average erosion rate of 0.7 m/a.

Figure 6b shows that after the coastal engineering construction, the southwest coastal segment including transects T01–T66 was eroded significantly at an average erosion rate of 3.2 m/a, and the maximum erosion occurred on transects T26 and T27 at a peak rate of 5.8 m/a. However, the northeastern segment including transects T67–T121 was significantly accreted at an average accretion rate of 8.5 m/a. Meanwhile, the accretion rates increased in the northeast direction, and the maximum accretion occurred in transect T121 at the northeast end at an accretion rate of 17.8 m/a. Thus, the shoreline evolution in the period 2006–2019 was characterized by significant erosion on the southwest beach and extremely significant accretion on the northeast beach. This indicates that beach rotation occurred during this period and that the rotation point was located between transects T66 and T67. Furthermore, based on a comparison with the results shown in Fig. 3, the spatial characteristics of the shoreline change rates from 2006 to 2019 were similar to those from 1986 to 2019, thus indicating that the shoreline changes in the past 13 years predominated the longer term (>30 years) evolution of Jing-

hai Bay. Additionally, shoreline rotation was caused by the construction of the shore-normal structure.

5 Discussions

The purpose of this study is to investigate the beach rotation caused by the construction of a shore-normal structure at the updrift headland of Jinghai Bay and to clarify the effect of the structure on shoreline evolution in the medium to long term. As shown in Fig. 4, the longshore characteristics of the shoreline change rates over the past 30 years indicate that the southwest beach eroded (at an average rate of 3.1 m/a), whereas the northeast beach accreted (at an average rate of 5.6 m/a). This opposing relationship between the two opposite ends of Jinghai Bay implies that the shoreline experienced clockwise rotation, with a rotation point located between transects T73 and T74. To further clarify whether this shoreline rotation was caused by the shore-normal structure, the M–K trend test method was performed, and the recent significant shoreline changes on 121 transects was identified to have commenced in early 2006 (September 2006). This indicates that the significant effect of coastal engineering on the shorelines occurred neither at the beginning nor at the end of the construction, but rather one year after the construction.

Based on the identified time, the shoreline evolution of Jinghai Bay over the past 30 years was classified into two periods (Fig. 6).

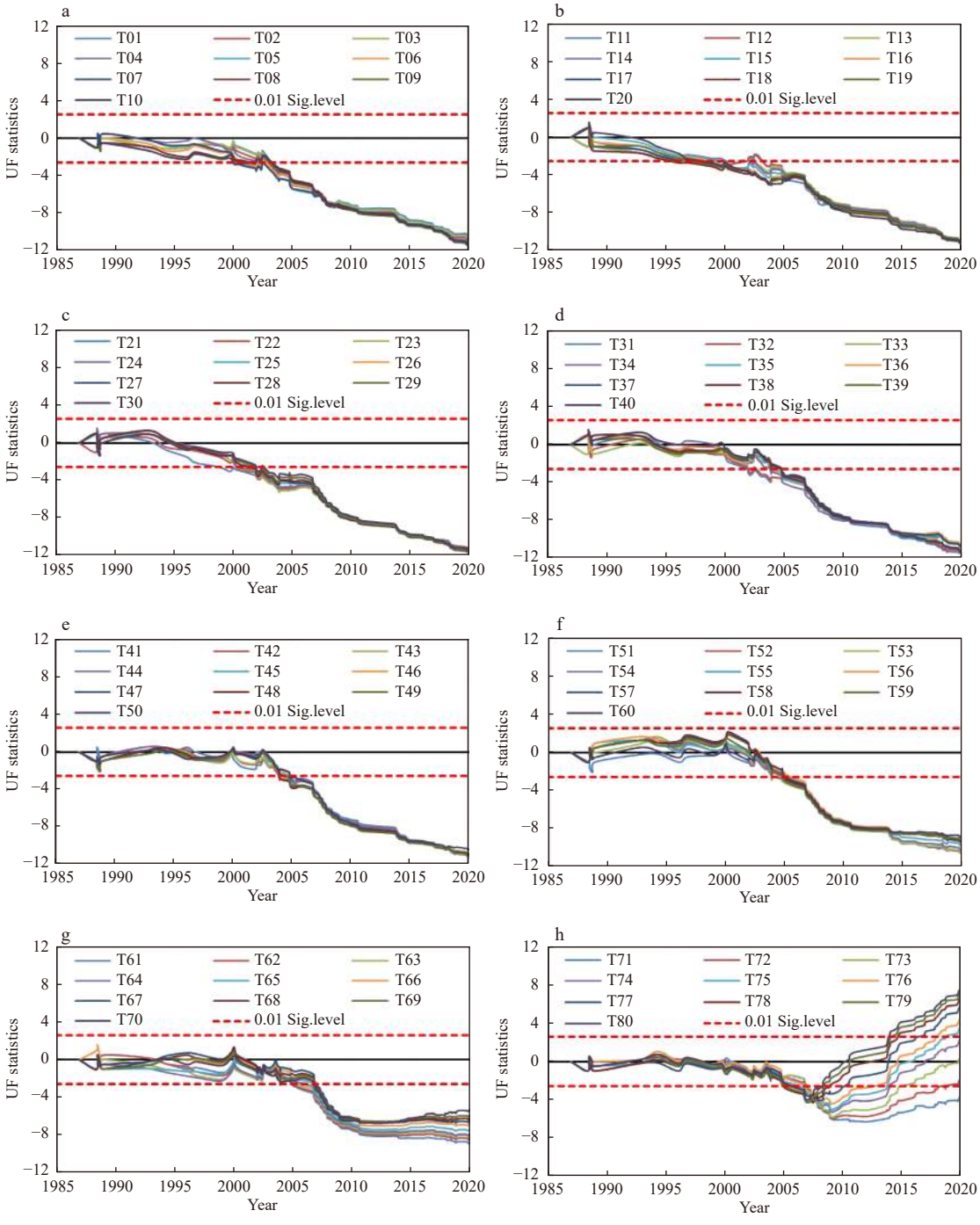

Fig. 5.

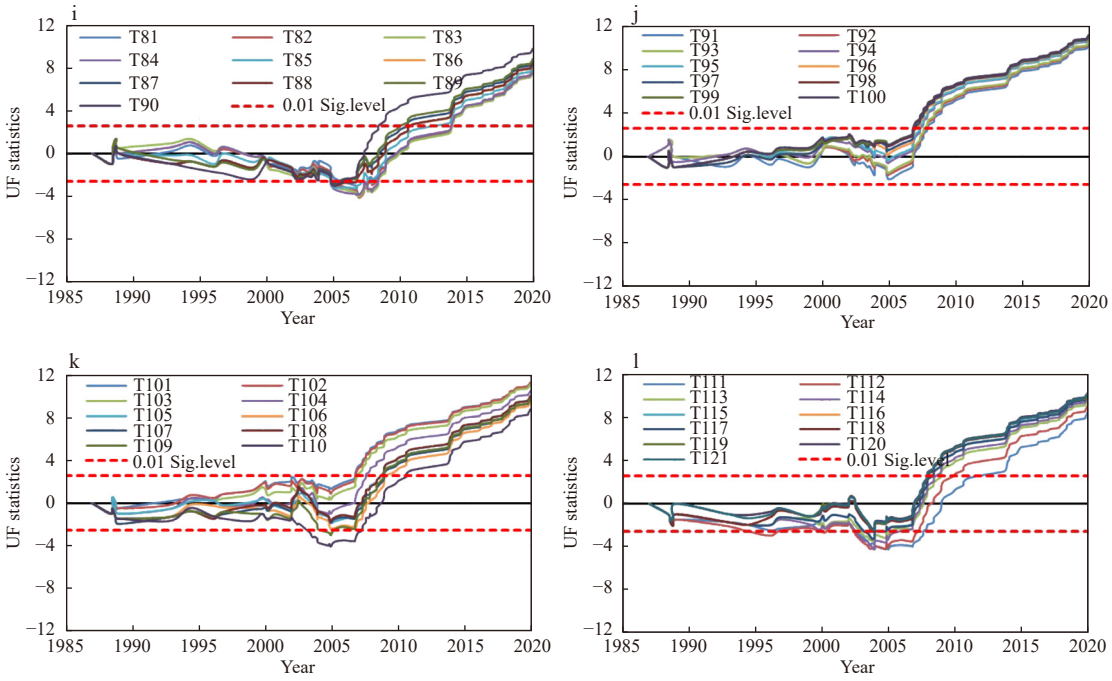

Fig. 5. Shoreline change trend and significance of specific transects based on M–K trend test.

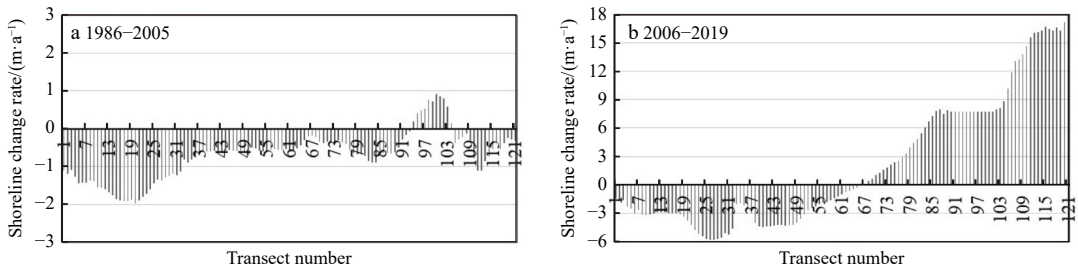

Fig. 6. Values of shoreline change rate calculated based on LRR at early and late periods.

Before the construction of the structure, 90.9% of the shorelines was eroded, and the average erosion rate of the entire bay was 0.7 m/a, thus indicating that slight erosion was the main feature of the shoreline evolution in the early period. However, after the construction of the structure, intense erosion with an average value of 3.2 m/a (maximum value of 5.8 m/a) occurred on the southwest beach, whereas significant accretion with an average value of 8.5 m/a (maximum value of 17.8 m/a) appeared on the northeast beach. This inverse relationship between the two opposite ends indicates that shoreline rotation occurred around a rotation point located between transects T66 and T67. By comparing the erosion and accretion conditions of different coastal segments in these two different periods, shoreline erosion accelerated on the southwest beach after the construction of the structure, whereas an opposite trend was indicated on the northeast beach. Therefore, coastal engineering project resulted in significant shoreline changes to Jinghai Bay, such as shoreline rotation. Furthermore, a comparison between the shoreline evolution characteristics after the construction of the structure (Fig. 6b) and those from 1986 to 2019 presented in Fig. 4 shows that the shoreline evolution over the past 30 years was primarily reflected by shoreline changes after the construction of the structure, which were represented by the clockwise rotation of the coastline. Our recent field observations of beach morphodynamics at Jinghai Bay on February 27, 2023 confirmed that this phenomenon continued (Fig. 7). Owing to the continued occurrence of erosion on the southwest beach, longshore seawalls and groins were constructed in the past two years to prevent the further erosion of this segment (Fig. 7a). By contrast, the northeastern beach featured a wide backshore with small dunes formed by aeolian processes (Fig. 7b).

Meanwhile, Ji et al. (2016) analyzed the changes in 2 m and 5 m isobaths of Jinghai Bay in 1966, 2003, 2008, and 2011 and highlighted that the shorelines of the sheltered northeast segment migrated landward, whereas the open southwest segment shifted seaward prior to the construction of the structure. However, after the construction, severe retreat occurred on the southwest beach, whereas rapid accretion occurred on the northeast beach. Additionally, they suggested that the direction of the longshore sediment transport was NE to SW before the construction of the structure, and SW to NE after the construction of the structure. Their results were consistent with the classic beach rotation model defined by Short and Masselink (1999), the coastline rotated anticlockwise and clockwise before and after the engineering construction, respectively. If a longshore exchange of sediment occurs between the two opposite ends of an embayed beach, then a significant wave direction shift (90° or greater in the dominant wave direction) will occur between the clockwise and

Fig. 7. Observations of beach morphodynamics at Jinghai Bay on February 27, 2023: a. southwest beach with newly-constructed seawalls and groins; b. northeast beach with wide backshore and aeolian dunes.

Fig. 8. Conceptual model of shoreline changes due to cross-shore/longshore sediment transport processes observed in this study: Before (a) and after construction of shore-normal structure (b). White arrows represent direction and magnitude of cross-shore sediment transport; blue arrow denotes direction of longshore sediment transport.

anticlockwise turns of the beach. However, the simulation results for the wave field before and after the engineering construction based on the CMC-Wave model did not reflect this significant shift in the wave direction (Ji et al., 2016). Meanwhile, the results of this study showed that before the construction of the structure (Fig. 6a), except for transects T94–T104 near the northeast end that were slightly accreted at an average rate of 0.6 m/a, most of the embayed coastline was subjected to erosion. This indicates that the changes in the 2 m isobath may not reflect the change in the actual shoreline, and that the seaward advance of the 2 m isobaths on the southwest beach is likely caused by the underwater accumulation of sediment eroded from the beach face.

Our results revealed that the construction of the shore-normal structure at the updrift headland of Jinghai Bay resulted in a clockwise shoreline rotation around the rotation point between transects T66 and T67, which was caused by the planform adjustment of the embayed beach in response to the varying positions of the wave diffraction point. Before the construction of the structure, the offshore transport of sediment mainly occurred in Jinghai Bay, particularly on the southwest beach, where the sediment eroded from the aerial beach and deposited in the nearshore zone owing to the direct incidence and impact of ESE and E waves on the exposed southwest beach (Ji et al., 2016). Additionally, Ji et al. (2016) simulated the wave field of Jinghai Bay after the construction of the structure using the CMS-Wave model and showed that ESE and E waves directly impacted the exposed southwest beach, thus causing the southwest beach to erode. However, these waves diffracted when passing through the shore-normal breakwater, thereby resulting in a significantly reduced wave energy on the northeast beach under the shelter of the breakwater; additionally, sediment was more likely to be deposited in the shelter zone. The results of this study indicate that after the construction of the structure, the clockwise rotation of the coastline of Jinghai Bay involved longshore sediment transport from southwest to northeast, which is consistent with the wave field simulation results of Ji et al. (2016). However, as shown in Fig. 6b, the accretion rates of the northeast beach were significantly higher than the erosion rates of the southwest beach, which indicates that more sediment accumulated on the aerial beach in the northeast of Jinghai Bay. This implies that the clockwise rotation of the coastline is not only related to longshore sediment transport from southwest to northeast, but also to cross-shore sediment transport processes. After the construction of the structure, because the shore-normal breakwater at the updrift headland extended sufficiently far offshore (1.2 km), the sheltered area increased significantly, whereas the wave height was reduced considerably. Such wave conditions contributed to onshore sediment transport processes, which resulted in an unusually high degree of accretion on the northeast beach (Fig. 7b). The aforementioned results were synthesized into a conceptual model incorporating cross-shore and longshore sediment transport processes before and after the construction of the shore-normal structure, as shown in Fig. 8. Our results were similar to those of studies pertaining to Narrabeen–Collaroy Beach in southeast Australia by Harley et al. (2011, 2015), who similarly indicated that although embayed beach rotation was assumed to be dominated by longshore sediment transport processes, the longshore variation in the cross-shore sediment transport processes might be more significant. In addition, the study area is located in a wave-dominated micro-tidal nearshore region (mean tide range <1 m). Our seven observations of beach morphodynamics in Jinghai Bay from 2015 to 2013 showed that the southwestern beach was primarily the barred beach morphodynamic type, whereas the northeastern beach was primarily reflective (Fig. 7). According to Davis (1985), tides impose adverse or indirect effects on sediment transport and beach morphology. Masselink and Short (1993) indicated that a large relative tidal range inhibited the formation of offshore bars. Therefore, the low tidal range was conducive to maintaining the barred beach morphodynamic type caused by the average wave conditions of the southwest beach and the linear beach face morphology of the northeast beach.

Owing to the barrier of the shore-normal breakwater to longshore sediment transport, the study area became a closed system after the construction of the structure, no long-term sediment gain or loss was indicated in the entire Jinghai Bay. This has been similarly observed at other locations worldwide (da Fontoura Klein et al., 2002; Harley et al., 2011). Additionally, the study of beach rotation by Short et al. (2000) indicated a rotation point with minimum variation, around which the beach rotated. da Fontoura Klein et al. (2002) investigated the short-term rotation processes of headland-bay beaches and suggested that the beach

rotated around a transition area. However, our study indicates that the rotation point of the beach caused by shore-normal engineering at the updrift headland was located between transects T66 and T67. Considering that the distance between the two transects was 50 m, one can assume that the beach rotated over a narrow area. However, because the amount of sediment deposited on the northeastern beach increases over time, one must observe whether the rotation point of the Jinghai coastline propagates in the southwest direction. Our results were similar to those of a study regarding headland-bay beaches in Tenby, West Wales by Thomas et al. (2010), who reported a steady northward migration of the rotation point.

In summary, many existing studies pertaining to beach rotation involved time-intensive beach profile observations over a long duration; however, the beach rotation phenomenon in our study was identified by constructing a time series of shoreline changes from all available Landsat satellite images since 1986. Currently, most studies pertaining to shorelines based on Landsat satellite remote sensing images are primarily based on a limited number of image data (Del Río et al., 2013; Xu and Gong, 2018; Zhang et al., 2021), which renders it difficult to assess the nonlinear behavior of beaches over a long duration and, therefore, to establish correlations with specific drivers. Hence, we extended the application of Landsat remote-sensing shoreline data. Nonetheless, we must be aware that the absence of long-term continuous observations pertaining to sandy beaches in China significantly restricts further studies related to beach processes. In this study, the shoreline position data obtained from six beach profile observations over the last five years were used to calculate the rates of shoreline change (Table 1) and were compared with those calculated after the construction of the structure based on remote sensing shoreline data from 2006 to 2019. The results indicated that the rate from the measured shoreline data for profile P01 was similar to that from the remote sensing shoreline data (corresponding to transect T40). However, significant differences were indicated in the shoreline change rates calculated from these two different data sources on other profiles, among which profile P04 showed not only different amplitudes of change, but also different directions of change. Therefore, long-term continuous observations of beach morphodynamics must be performed such that coastal processes and mechanisms in China can be investigated more comprehensively.

Table 1. Comparison of shoreline change rates calculated via LRR using measured shoreline data in the last five years and remote sensing shoreline data from 2006 to 2019

Measured profiles	Corresponding transects	Rates from measured profile data/(m·a^{-1})	Rates from remote sensing shoreline data/(m·a^{-1})
P01	T40	−4.3	−4.5
P02	T47	−2.1	−4.3
P03	T60	−3.0	−1.2
P04	T69	−2.8	0.7
P05	T80	1.2	4.4
P06	T90	0.6	7.7

6 Conclusions

In this study, high-tide shorelines extracted from 87 Landsat satellite images from 1986 to 2019 were used to examine the medium-term to long-term shoreline evolution under the effect of a shore-normal structure at the updrift headland of Jinghai Bay, eastern Guangdong Province. Based on the LRR, the results indicated that erosion occurred in the southwest segment of the bay over the past 30 years at an average erosion rate of 3.1 m/a, whereas significant erosion occurred in the northeast segment at an average accretion rate of 5.6 m/a. To further determine whether this difference between the two opposite ends of the bay was caused by the shore-normal structure, we performed the M–K trend test to identify significant trend changes for all 121 transects, that occurred in early 2006. Subsequently, the findings were categorized into those: before and after the construction of the structure. The results showed that the shorelines at Jinghai Bay were characterized by slight erosion, with an average erosion rate of 0.7 m/a before the construction of the shore-normal structure (1986–2005). However, significant erosion with a mean erosion rate of 3.2 m/a occurred on the southwest beach, whereas significant accretion with a mean accretion rate of 8.5 m/a occurred on the northeast beach after the construction (2006–2019). The results revealed that the shore-normal structure at the updrift headland resulted in a clockwise rotation of the shorelines. Further analysis indicated that after the construction of the structure, the clockwise rotation of the shorelines was not only promoted by the longshore sediment transport processes from southwest to northeast, but was also involved in the cross-shore sediment transport processes. Using all available Landsat satellite image data from Jinghai Bay since 1986, we elucidated the beach rotation caused by the shore-normal structure. The results of this study are crucial for beach erosion risk management, coastal disaster zoning, regional sediment budget assessments, and further observations and predictions of beach morphodynamics.

References

Anthony E J, Gardel A, Dolique F, et al. 2002. Short-term changes in the plan shape of a sandy beach in response to sheltering by a nearshore mud bank, Cayenne, French Guiana. Earth Surface Processes and Landforms, 27(8): 857–866, doi: 10.1002/esp.357

Benkhattab F Z, Hakkou M, Bagdanavičiūtė I, et al. 2020. Spatial-temporal analysis of the shoreline change rate using automatic computation and geospatial tools along the Tetouan coast in Morocco. Natural Hazards, 104(1): 519–536, doi: 10.1007/s11069-020-04179-2

da Fontoura Klein A H, Benedet Filho L, Schumacher D H. 2002. Short-term beach rotation processes in distinct headland bay beach systems. Journal of Coastal Research, 18(3): 442–458

Davis R A Jr. 1985. Beach and nearshore zone. In: Davis R A, ed. Coastal Sedimentary Environments. 2nd ed. New York: Springer, 379–444

Del Río L, Gracia F J, Benavente J. 2013. Shoreline change patterns in sandy coast. A case study in SW Spain. Geomorphology, 196: 252–266, doi: 10.1016/j.geomorph.2012.07.027

Dolan R, Fenster M S, Holme S J. 1991. Temporal analysis of shoreline recession and accretion. Journal of Coastal Research, 7(3): 723–744

Fenster M S, Dolan R. 1994. Large-scale reversals in shoreline trends along the U. S. mid-Atlantic coast. Geology, 22(6): 543–546, doi: 10.1130/0091-7613(1994)022<0543:LSRIST>2.3.CO;2

Hansen J E, Barnard P L. 2010. Sub-weekly to interannual variability of a high-energy shoreline. Coastal Engineering, 57(11-12): 959–972, doi: 10.1016/j.coastaleng.2010.05.011

Harley M D, Turner I L, Short A D, et al. 2011. A reevaluation of coastal embayment rotation: the dominance of cross-shore versus alongshore sediment transport processes, Collaroy-Narrabeen Beach, southeast Australia. Journal of Geophysical Research:Earth Surface, 116(F4): F04033

Harley M D, Turner I L, Short A D. 2015. New insights into embayed beach rotation: the importance of wave exposure and cross-

shore processes. Journal of Geophysical Research:Earth Surface, 120(8): 1470–1484, doi: 10.1002/2014JF003390

Hou Xiyong, Wu Ting, Hou Wan, et al. 2016. Characteristics of coastline changes in mainland China since the early 1940s. Science China Earth Sciences, 59(9): 1791–1802, doi: 10.1007/s11430-016-5317-5

Ji Hongyu, Chen Shenliang, Lei Yaping, et al. 2016. Effects of engineering on coastal morphodynamic evolution of Jinghai Bay in Southern China. The Ocean Engineering (in Chinese), 34(5): 57–64

Kendall M G. 1975. Rank Correlation Methods. 4th ed. London: Charles Griffin

Li Zhilong, Chen Zishen. 2006. Equilibrium shape model of headland-bay and application in South China coasts. Journal of Oceanography in Taiwan Strait (in Chinese), 25(1): 123–129

Mann H B. 1945. Nonparametric tests against trend. Econometrica, 13(3): 245–259, doi: 10.2307/1907187

Masselink G, Pattiaratchi C B. 2001. Seasonal changes in beach morphology along the sheltered coastline of Perth, Western Australia. Marine Geology, 172(3-4): 243–263, doi: 10.1016/S0025-3227(00)00128-6

Masselink G, Short A D. 1993. The effect of tide range on beach morphodynamics and morphology: a conceptual beach model. Journal of Coastal Research, 9(3): 785–800

Maune D F. 2007. Digital Elevation Model Technologies and Applications: The DEM Users Manual. 2nd ed. Bethesda, Maryland: American Society for Photogrammetry and Remote Sensing, 1–655

Ojeda E, Guillén J. 2008. Shoreline dynamics and beach rotation of artificial embayed beaches. Marine Geology, 253(1-2): 51–62, doi: 10.1016/j.margeo.2008.03.010

Ranasinghe R, McLoughlin R, Short A D, et al. 2004. The Southern Oscillation Index, wave climate, and beach rotation. Marine Geology, 204(3-4): 273–287, doi: 10.1016/S0025-3227(04)00002-7

Short A D, Masselink G. 1999. Embayed and structurally controlled beaches. In: Short A D, ed. Handbook of Beach and Shoreface Morphodynamics. New York: John Wiley, 230–250

Short A D, Trembanis A C. 2004. Decadal scale patterns in beach oscillation and rotation Narrabeen beach, Australia—Time series, PCA and wavelet analysis. Journal of Coastal Research, 20(2): 523–532

Short A D, Trembanis A C, Turner I L. 2000. Beach oscillation, rotation and the southern oscillation, Narrabeen Beach, Australia. In: Proceeding of 27th International Coastal Engineering Conference. Sydney: ASCE, 2439–2452

Thieler E R, Himmelstoss E A, Zichichi J L, et al. 2017. The Digital Shoreline Analysis System (DSAS) version 4.0–An ArcGIS extension for calculating shoreline change. Reston: U. S. Geological Survey, 49–50

Thomas T, Phillips M R, Williams A T. 2010. Mesoscale evolution of a headland bay: Beach rotation processes. Geomorphology, 123: 129–141, doi: 10.1016/j.geomorph.2010.06.018

Thomas T, Phillips M R, Williams A T, et al. 2011a. A multi-century record of linked nearshore and coastal change. Earth Surface Processes and Landforms, 36(8): 995–1006, doi: 10.1002/esp.2127

Thomas T, Phillips M R, Williams A T, et al. 2011b. Short-term beach rotation, wave climate and the North Atlantic Oscillation (NAO). Progress in Physical Geography:Earth and Environment, 35(3): 333–352, doi: 10.1177/0309133310397415

Wei Fengying. 2007. Statistical Diagnosis and Prediction Technique of Modern Climate (in Chinese). 2nd ed. Beijing: China Meteorological Press, 69–72

Xu Nan, Gong Peng. 2018. Significant coastline changes in China during 1991-2015 tracked by Landsat data. Science Bulletin, 63(14): 883–886, doi: 10.1016/j.scib.2018.05.032

Yu Jitao, Chen Zishen. 2011. Study on headland-bay sandy coast stability in South China coasts. China Ocean Engineering, 25(1): 1–13, doi: 10.1007/s13344-011-0001-1

Zhang Xiang, Wang Xiaopeng, Huang Anqi, et al. 2021. Extraction of complex coastline feature and its multi-year changes in Shandong Peninsula based on remote sensing image. Transactions of Oceanology and Limnology (in Chinese), 43(2): 171–181

Zhu Luoyun, Liu Tingting, Fan Renfu, et al. 2022. Study on the evolution process and driving mechanism of the sandy shoreline of the Qiwang Bay in eastern Guangdong from 1986 to 2019. Haiyang Xuebao (in Chinese), 44(7): 82–94